Relaxivity assessment and T1 mapping of ex vivo lymph nodes

Nuhamin Valk
s2485990

Supervisors: Dr.ir. L. Alic, dr.ir. F.F.J. Simonis, dr.ir. F. Ayatollahi

Magnetic Detection & Imaging Department
University of Twente
The Netherlands

Abstract

Background: Breast cancer is the most prevalent cancer in Dutch women. A strong prognostic determinant is spread to the axillary lymph nodes, which can be determined using a sentinel lymph node biopsy (SLNB). This procedure uses radioactive tracers, although alternative magnetic tracers have been proposed, which are shown to be non-inferior and solve some of the issues associated with the use of radioactive materials. However, the need remains to remove the lymph node in order to assess the presence on metastases. MR mapping and evaluation could possibly provide a method to do this in vivo.
Goal: Determine the relaxivity of the magnetic tracer used in SLNBs and create T_1 maps of ex vivo lymph nodes of breast cancer patients, which can be used to evaluate lymph nodes on the presence of metastases.
Method: To determine the tracer relaxivity, MRI data from various samples containing different concentrations of the tracer diluted in water was used. The relaxivity was then determined by the slope of the fit through the differences in R_1 between the sample and water against the sample concentration. To create the T_1 map, MRI data from a breast cancer patient that underwent an SLNB using a magnetic tracer was used. T_1 was determined for each voxel by fitting signal intensities against inversion times. The results were mapped and analyzed on the goodness of fit.
Results: Measurements of the same sample resulted in deviations in the measured T_1 and the final relaxivity was determined as 15.4 $s^{-1}mM^{-1}$. Mapping of the lymph node generally lead to a good goodness of fit.
Discussion: The tracer samples were not held at a constant temperature, which could explain the deviations in T_1. It was not possible to map every voxel on every slice on the lymph node; data initialization and regularization is needed to improve the applicability of the fit. Furthermore, a quantitative analysis of the tracer concentration in a lymph node is prevented by the absence of a T_1 map done prior to tracer admission, which is needed to calculate the difference in R_1 caused by the tracer.
Conclusion: This research provides the relaxivity of a magnetic tracer used in SLNBs and a method to acquire a T_1 map of a lymph node. Further research is needed to overcome the lack of native T_1 map, to increase the applicability of the fit by data initialization and regularization, and to analyze differences in magnetic properties and tracer uptake between lymphatic and metastatic tissue, so that quantitative assessment of the tracer concentration and evaluation on the presence of metastases using MRI could one day be possible.

Samenvatting

Achtergrond: Borstkanker is de meest voorkomende kankersoort bij Nederlandse vrouwen. Een laksd;flaksd is uitzaaiing naar lymfeknopen in de oksels, wat kan worden gediagnosticeerd aan de hand van een schildwachtklierprocedure. Hierin worden radioactive tracers gebruikt, maar er zijn alternatieve magnetische tracers voorgesteld die niet-inferieur zijn aan radioactive tracers en enkele problemen geassocieerd met radioactieve stoffen oplossen. Echter, de schildwachtklier moet in beide vallen worden verwijderd om op de aanwezigheid van uitzaaiingen te controleren. MR mappen en evaluatie zouden mogelijk gebruikt kunnen worden voor een in vivo methode hiervoor.
Doel: De *relaxivity* van de tracer bepalen en T_1 maps maken van ex vivo lymfeknopen van borstkankerpatiënten, die gebruikt kunnen worden om lymfeknopen te evalueren op de aanwezigheid van uitzaaiingen.
Methode: Voor het bepalen van de *relaxivity* is MRI data afkomstig van monsters met verschillende tracerconcentraties in water gebruikt. De *relaxivity* was vervolgens bepaald door de helling van de fit door de verschillen in R_1 uitgezet tegen de concentratie te bepalen. Voor het maken van de T_1 maps is MRI data van een lymfeknoop van een borstkankerpatiënt gebruikt die is verwijderd als onderdeel van een schildwachtklierprocedure. T_1 is voor iedere voxel bepaald door de signaalintensiteiten te fitten tegen de inversietijden. De resultaten zijn gemapt en geanalyseerd op de juistheid van de fit.
Resultaten: Metingen aan monsters met dezelfde concentraties gaven verschillen in T_1 en de uiteindelijke *relaxivity* kwam uit op 15.4 $s^{-1}mM^{-1}$. Het mappen van de lymfeknoop leidde in het algemeen ook tot een goede fit.
Discussie: De tracermonsters hadden geen constante temperatuur, wat de variaties in de gemeten T_1 mogelijk verklaart. Het was niet mogelijk om elke voxel op elke slice van elke lymfeknoop te bepalen; data initialisatie en regularisatie is nodig om de toepasbaarheid van de fit te vergroten. Verder is een kwantitatieve analyse van de tracerconcentratie in een lymfeknoop niet mogelijk, doordat T_1 mappen niet mogelijk is voorafgaand aan het toedienen van een tracer, wat nodig is om het verschil in R_1 te kunnen berekenen.
Conclusie: Dit onderzoek heeft de *relaxivity* van een magnetische tracer die wordt gebruikt voor een schildwachtklierprocedure. Verder onderzoek is nodig om een oplossing te vinden voor het missen van een pre-tracer T_1 map, om de toepasbaarheid te vergroten door data initialisatie en regularisatie en om verschillen in magnetische eigenschap tussen gezond lymfeweefsel en tumorweefsel in kaart te brengen. Zo kan in de toekomst mogelijk de tracerconcentratie kwantitatief worden bepaald en kan de aanwezigheid van uitzaaiingen aan de hand van MRI worden geëvalueerd.

Contents

1 Introduction

One in seven women in the Netherlands gets diagnosed with breast cancer at some point in her life, making it by far the most prevalent cancer in women. [1] Accurate staging of the cancer is crucial, as the survival rate depends highly on the stage at diagnosis. [2]

Metastatic spread to the axillary lymph nodes is a strong prognostic determinant in early stage breast cancer. The sentinel lymph node (SLN) is in turn the first node in the lymphatic basin that receives lymphatic drainage from the breast, and thus the most likely location for potential metastases. The presence of metastases in the SLN thus indicates that there is a possibility of metastases in other axillary lymph nodes. [3, 4, 5, 6]

1.1 Sentinel lymph node biopsy

To determine whether or not the cancer could have spread from the primary tumor to the axillary lymph nodes, the presence of metastases in the SLN needs to be assessed. This is done by a sentinel lymph node biopsy (SLNB), which is currently the standard surgical procedure in staging breast cancer. [7] During this procedure, a radioactive marker is first administered close to the tumor. Then, the SLN is identified using a radioactive detector. Finally, the SLN is removed and assessed on the presence of metastases. [8]

An SLNB comes with fewer side effects and is less invasive than an axillary lymph node dissection, the previous routine procedure to stage breast cancer, during which more than one lymph node is removed. [9, 10, 11] An SLNB also has a high accuracy (90 to 95%) and a low false-negative rate (5 to 15%). [7]

However, there are still some disadvantaged that come with an SLNB. First of all, in around three quarters of patients on which an SLNB is performed, no metastases are present in the SLN. [12, 13] In those cases, an SLNB would not have to be performed if the presence of metastases could be determined in vivo pre-operatively. This could prevent side effects, such as lymphedema, seroma, and difficulties with moving the arm, and reduce the amount of unnecessary surgeries that are performed. [14] Second, as there are only a few reactors that produce the isotope necessary for the radioactive tracer, the supply of the tracer is highly susceptible to shortages. [15] Furthermore, radioactive substances require specific regulatory requirements and special handling by clinicians. [16]

1.2 Magnetic tracers

Alternative tracers, e.g. super-paramagnetic iron oxide nanoparticles (SPION) based tracers such as Magtrace, are used to overcome the disadvantages that come with using radioactive tracers. [16] These have been shown to be non-inferior in detecting SLNs. [8, 17] However, there is no general method to detect metastases in SLNs in vivo pre-operatively, so still many non-metastatic lymph nodes are removed from patients, resulting in unnecessary surgeries and side effects. [18] If pre-operative in vivo detection of metastases in SLNs were possible, it would remove the need for an SLNB in the case of a negative node, resulting in a drastic decrease in the amount of SLNBs that need to be performed.

1.3 Aim and goal

Therefore, the aim of this research is to find a method to assess the presence of metastases in sentinel lymph nodes using Magnetic Resonance Imaging and the tracer containing SPIONs. The goal of this paper is to quantitatively assess the SPION concentration in ex vivo lymph nodes of breast cancer patients using a T_1 map, which could possibly be used to distinguish healthy lymphatic tissue from metastases. This leads to the following research question: **How can the SPION concentration in an ex vivo LN be determined, using a T1 map?** This question will be answered in two parts:

- What is the relaxivity of the magnetic tracer Magtrace?
- How can T_1 of voxels of a lymph node be determined and visualized?

2 Theoretical background

2.1 Principles of MRI

Magnetic resonance imaging (MRI) is an imaging method which uses the spin characteristics of nuclei to picture, among other things, human tissues. Nuclear spins can be visualized as a planet rotating around its own axis with a north and south pole and usually these spins do not have a preferred direction. However, when a magnetic field (B_0) is applied on a spin system, the preferred orientation becomes parallel or anti-parallel to the externally applied magnetic field. This is called nuclear magnetism. [19]

The spins in a magnetic field can be averted away from their alignment with the externally applied magnetic field by applying energy as radiofrequency (RF) pulses at the resonance or Larmor frequency of the spins. This extra energy causes the some spins to occupy a higher energy state and causes the net magnetization of the spin system to flip 90°: from the positive z-axis to the transverse xy-plane. When the RF pulse is eventually turned of, the spins return to their lower energy equilibrium state, aligned with the external magnetic field. This process is called longitudinal- or T_1 relaxation.[19, 20, 21, 22]

Spins need to lose some of their energy to return to the lower energy equilibrium state, and they do so by transferring heat to their surroundings. [23] Therefore, the T_1 relaxation time, which is defined as the time it takes for the magnetization to return to 63% of its equilibrium value, depends on how easily the spin system can exchange energy with its surroundings. For example, molecules that rotate quickly, such as liquids, have longer T_1 times than slower moving molecules, such as solids, as more rapidly moving molecules contain more kinetic energy and thus cannot absorb energy as easily as slower moving molecules. [23]

The magnetic spins that form the longitudinal magnetization gain energy when an RF pulse is applied. So, to return to the equilibrium state, the spin system needs to lose some of its energy to its surroundings. T_1 thus depends on how easily the spin system can exchange energy with its environment. For example, a large temperature difference between the excited tissue and the surrounding tissue allows for an easier exchange of energy and thus for a shorter relaxation time.

The time it takes for the magnetization to return to 63% of its equilibrium value is defined as the longitudinal relaxation time, also known as the T_1 relaxation time (Figure 1. [24] A short T_1 indicates that the magnetization recovers quickly, a long T_1 means a slow recovery. [19] The signal intensity during T_1 relaxation is described by Equation 1, which shows how the signal intensity depends on the inversion time and the longitudinal relaxation time for a certain equilibrium value of the spins in the case of an inversion recovery spin echo sequence (Section 2.2.1). [19, 25] The Equation describes logarithmic growth; as time passes by, the surroundings take up more and more energy from the system, thus it becomes harder for the spins to pass on energy to their surroundings, resulting in a decline in the rate at which recovery occurs. The parameter a causes the graph to go through the origin, M_0 is the magnetization at equilibrium. [24, 19]

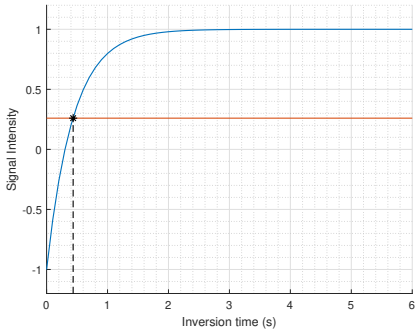

Figure 1: *Graph of the function for signal intensity against inversion time in the case of an inversion recovery spin echo sequence (Section 2.2.1). The blue line shows the function that describes the signal intensity as a function of the inversion time in seconds after an inversion pulse. The red line represents the signal intensity at 63%. The time at the intersection between these lines is defined as T_1, as the signal intensity has recovered to 63% of its initial value by that time. The signal intensity is normalized between -1 and 1.*

$$SI = M_0(1 - 2e^{\frac{-TI}{T1}}) + a \tag{1}$$

2.2 MR mapping

2.2.1 Data acquisition: inversion recovery spin echo sequence

The inversion recovery spin echo (IRSE) sequence is an MRI sequence that is comprised of two pulses separated by an inversion time (TI). The first pulse in a 180° RF-pulse that inverts the longitudinal magnetization M_z. After this pulse, the magnetization recovers.. Then, after TI has passed, a second, 90° RF-pulse, flips the longitudinal magnetization into the transverse plane. After this pulse, the signal intensity is measured. Repeating this for various known TIs and fitting the acquired data to Equation 1 is used to determine the longitudinal relaxation time of materials and tissues. [26]

2.2.2 T_1 mapping

A T_1 map shows the absolute pixel-wise T_1 relaxation time of an object or tissue. [27] Mapping is, contrary to T_1 weighted imaging, a quantitative technique, as it does not show relative intensities of tissues, but their absolute relaxation times. T_1 mapping is, for example, used in cardiology. Some cardiac diseases are characterized by a change in T_1, but these changes are sometimes diffuse and thus difficult to detect using T_1 weighted imaging, where only the relative signal intensities are shown. T_1 mapping does allow for detection of these changes, as the T_1 of tissues is visualized and it can be compared to the T_1 of healthy tissue. [22]

T_1 maps are created by measuring the magnetization - the signal intensity - at various TIs. Next, Equation 1 is fitted through these data points, from which T_1 is derived. This is done for all the voxels in the field of view. T_1 can then be visualized using a color-encoded map.

2.3 Superparamagnetic iron oxide nanoparticles

Superparamagnetic iron oxide nanoparticles (SPIONs) are particles which superparamagnetic properties cause field pertubations in an external magnetic field. [28] These effects shorten the relaxation time of nearby spins, because their local magnetic fields are much stronger than that of nuclear spins, accelerating the spin lattice relaxation. Therefore, tissues containing SPIONs will have a shortened T_1 compared to tissues without. [29] These properties make SPIONs suitable to function as MRI contrast agents or tracers.

2.3.1 Relaxivity

The degree of enhancement of the longitudinal relaxation rate caused by a MRI contrast agent (CA) or tracer is called the relaxivity. This degree of enhancement depends on the concentration, among other things, so it is normalized to the concentration. Equation 2 demonstrates the relation between the relaxation time, relaxation rate and the relaxivity. R_1 is the relaxation rate ($R_1 = 1/T_1$), $T_1(C)$ is the relaxation time for a certain concentration of tracer or CA, ${T_1}^0$ is the native relaxation time, T_1 in absence of the tracer, r_1 is the relaxivity, and C is the concentration of the tracer or CA. [30]

$$R_1(C) = \frac{1}{T_1(C)} = \frac{1}{T_1^0} + r_1 C \tag{2}$$

The relaxivity is equal to the slope of the graph plotting the difference in relaxivity between the native and post contrast relaxation rate against the tracer concentration, which is shown by rewriting Equation 2 into Equation 3. [30] So, by measuring the relaxation times using an IRSE at various concentrations, subtracting ${T_1}^0$ from the measured values, and fitting a linear equation through the plotted data points and through the origin, the relaxivity of a tracer can be determined.

$$r_1 = \frac{\Delta R_1}{C} \tag{3}$$

2.3.2 Relaxivity measurements

T_1 recovery follows a logarithmic growth curve, so the TIs at which the signal intensity is measured are usually logarithmically spaced, as the change in signal intensity is largest during the first moments of recovery (Figure 1, Equation 1). [31, 32, 33] There is, however, some dissensus on the optimal number of TIs at which the signal intensity is measured. More TIs lead to a more accurate determination of T_1, but more measurements do lead to a longer acquistion time. Henoumont, et al. state that "twelve time points adequately distributed along the whole curve are usually sufficient" [33]. However, Ogg, et al. state that "the precision of the T_1 estimate improved with [a] decreasing [number of] time points for $T_1 > 500$ ms", with an optimum for four data points [34]. Moreover, Bain expresses that "for the inversion-recovery experiment, experience shows that as long as the values are reasonable (i.e., in the range 0-2 T_1), the experiment gives useful, reliable results. In other words, the results are not strongly dependent on the choice of T_1, so the experiment is very robust." [32].

The repetition time (TR) should allow for the signal intensity to return to its equilibrium value, so it must be longer than T_1, but a large TR does increase the acquistition time. Taking five times the estimated T_1 value as TR allows for 98.5% to complete relaxation and a reasonable acquisition time in the case of a reasonable estimation. [33, 35]

To determine the relaxivity, T_1 in absense and presense of a CA or tracer, a T_1 map is acquired prior to and after its admission. In in vitro experiments, this is done by mapping the diluted sample and the used solvent, where the map of the solvent represents the situation before admission of a tracer or CA. [31] In in vivo experiments, the maps of the situation before and after admission of the CA or tracer are acquired. [36, 37]

2.3.3 Applicability on determining SPION concentration in ex vivo SLNs

There is a big issue that arises when the previously described methods of T_1 are applied when determining the SPION concentration in ex vivo SLNs. The concentration calculations require a difference in relaxation rates before and after admission of the tracer. However, in the context of a SLNB, where ex vivo SLNs are mapped, it is impossible to acquire a ${T_1}^0$ map, so the concentration of a voxel cannot be determined using the relaxivity of the tracer

Taking a T_1 from literature is also not possible, because the lymph nodes might contain metastases, which can alter the relaxation time of the tissue. This approach would also require detailed knowledge on the type of lymphatic tissue each voxel contains, as the relaxation times of the LN cortex, hilum and lymphatic fluid can differ greatly, at least at 3.0T. [38, 39] There was no literature found on the relaxation times at 0.5T, but it can be assumed that T_1 differs for different lymphatic tissues at this field strength as well.

3 Relaxivity measurements of the Magtrace magnetic tracer

3.1 Method

3.1.1 Creating solutions with different SPIO concentrations

To determine the relaxivity, the relaxation time has to be measured at various tracer concentrations. For these measurements, five different concentrations were used.

Magtrace consists of 28 mg iron per ml in the form of iron oxide, and 32 mg carboxydextran ($C_{19}H_{32}O_{18}$) per ml. [40, 41, 42] There was no further information found on the type of iron oxide in the tracer, and on the molecular structure of the coated particles. Because the molarity of the coated iron particles cannot be calculated with the available information, all the relaxivity calculations will be made using the molarity of iron. The assumption is made that Magtrace consists of 28 mg iron atoms per ml tracer with a molar mass of 55.845 g/mole, and based on this the molarity of iron is calculated. [43] This may not be the same as the molarity of the coated particles in the tracer, but this way the Magtrace concentration can be calculated from the slope of the graph of the relaxation rates against the molarity.

The investigated solutions have a concentration ranging from 0 to 1% Magtrace diluted in saline solution, to keep the NaCl concentration comparable to that of undiluted Magtrace. [40, 41] The volumes of Magtrace and saline solution , and the molarity of iron of each solution are shown in Table 1.

Table 1: *Volume of injection and of Magtrace considering a 1 ml lymph node for different uptakes*

% Magtrace	1%	0.75%	0.5%	0.25%	0%
volume Magtrace	150 µl	113 µl	75 µl	37.5 µl	0 ml
volume saline	14.85 ml	14.887 ml	14.925 ml	14.9625 ml	15 ml
molarity iron	5.014 mM	3.760 mM	2.507 mM	1.253 mM	0 mM

The relaxation rate of the tube containing just water is used as a native relaxation rate (R_1^0). However, in the case of a lymph node that was removed as part of an SLNB, no native T_1 and R_1 are available and thus the difference in relaxation rate cannot be calculated and used to determine the concentration. A way to circumvent this is by calculating the concentration using only R_1, but this inevitably leads to an error in the calculated concentration. To investigate the magnititude of this error, the concentration of each tube is determined using the corresponding relaxation rate and the resulting error is evaluated.

3.1.2 Data acquisition

The MR data was acquired using a 0.5 T MagSpec tabletop scanner from Pure Devices© (GmbH, Rimpar, Germany). The scanner operates at around 37° Celcius. A 0D, so one voxel, IRSE sequence was used, with TR set as five times the estimated T_1, as TR has to be sufficiently long to assure that the magnetizaton can return to equilibrium (Figure 2. [33, 35, 44] T_1 was measured four times for each solution. The first measurement was a test measurement to ensure T_1 estimated was chosen correctly and the resulting T_1 is not used to determine the relaxivity, only to determine T_1 estimated for the following three scans. The T_1 values that resulted from those scans were used to determine the relaxivity.

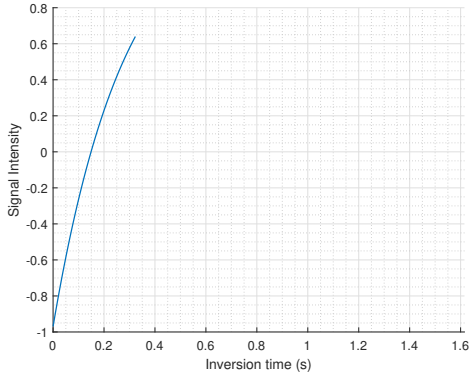

(a) *Longitudinal relaxation when TR is set as less than five times the estimated T_1. The magnetization does not return to its equilibrium value during this time frame.*

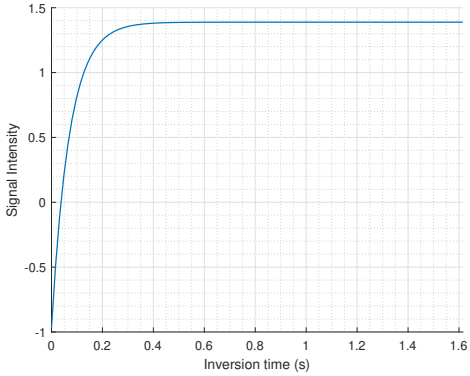

(b) *Longitudinal relaxation when TR is set as five times the estimated T_1. Enough time has passed for the magnetization to return to its equilibrium value.*

Figure 2: *Longitudinal relaxation in the case of a T_1 that is too short and a T_1 that is adequately chosen.*

T_1 was fitted to the acquired immediately after the data was. This was done using a single-exponential fitting algorithm from Pure Devices© in MATLAB. [45]

Twelve logarithmically spread TIs were used, as proposed by Henoumont, et al. [33] These TIs range from one tenth of T_1 estimated to thirty times T_1 estimated. Increasing TI logarithmically prevents undersampling of the signal without causing a undesirably long acquisition time. [44]

The field of view (FOV) was set as 15 by 15 by 15 mm, which is equal to the diameter of the tube.
The tubes were scanned in order of increasing Magtrace concentration, because it is expected that T_1 decreases as the concentration increases. A test scan was done for each tube with the T_1 of the previously scanned tube as T_1 estimate. The T_1 that resulted from this first test was then used as T_1 estimated for the next three scans. This way, a T_1 estimated and TR that did not allow for the equilibrium magnetization to be reached during the IRSE were prevented. For the first scan with the rube containing just the saline solution however, the T_1 time of water at 1.5 T was used as T_1 estimated, as there was no information found on the relaxation time of water at 0.5 T. Moreover, if T_1 is not in the range of T_1 estimated, T_1 estimated has to be adjusted to include T_1 and the data acquisition has to be redone. [25]

3.1.3 Data processing

The data was fitted using a linear equation through the origin (Equation 4). The resulting slope (r_1) is equal to the relaxivity. For each T_1 measurement, R_1 was determined by taking one over T_1. Then, ΔR_1 was calculated by subtracting the native R_1 from R_1. Finally, the relaxivity curve was fitted using a first degree polynomial fit through the origin, and r_1 was determined by taking the slope of the resulting graph.

$$SI = r_1 * TI \tag{4}$$

3.2 Results

Table 2 shows the average T_1, and the corresponding R_1 values for the different tracer concentrations. Several things stand out. First, ΔR_1 does not continuously increase linearly as the concentration increases, as would be expected. Instead, ΔR_1 increases more or less linearly up until 0.75%, between 0.75% and 1% it hardly increases. Also, the measurements at 3.760, 2.507, 1.253, and 0 mM (0.75%, 0.5%, 0.25%, and 0%, respectively) all have large error margins, especially in comparison to the measurements at 1%.

Table 2: *Average relaxation times and relaxivity rates for different Magtrace concentrations*

% Magtrace	Iron concentration (mM)	T_1 (ms)	R_1 (ms^{-1})	ΔR_1 (ms^{-1})
1%	5.014	14.3 ± 0.2	0.0698 ± 0.0010	0.065
0.75%	3.760	16.3 ± 3.1	0.0612 ± 0.0129	0.0609
0.5%	2.507	21.4 ± 3.0	0.0467 ± 0.0068	0.0463
0.25%	1.253	46.6 ± 7.7	0.0215 ± 0.0039	0.0211
0%	0	2832 ± 891	0.0353e-2 ± 0.0147e-2	0

Figure 3 shows the longitudinal relaxation rates plotted against the concentration and the linear fit to the relaxation rates. The fit has an adjusted R^2 of 0.9150. The resulting relaxivity (r_1) is equal to 15.4 $s^{-1}mM^{-1}$.

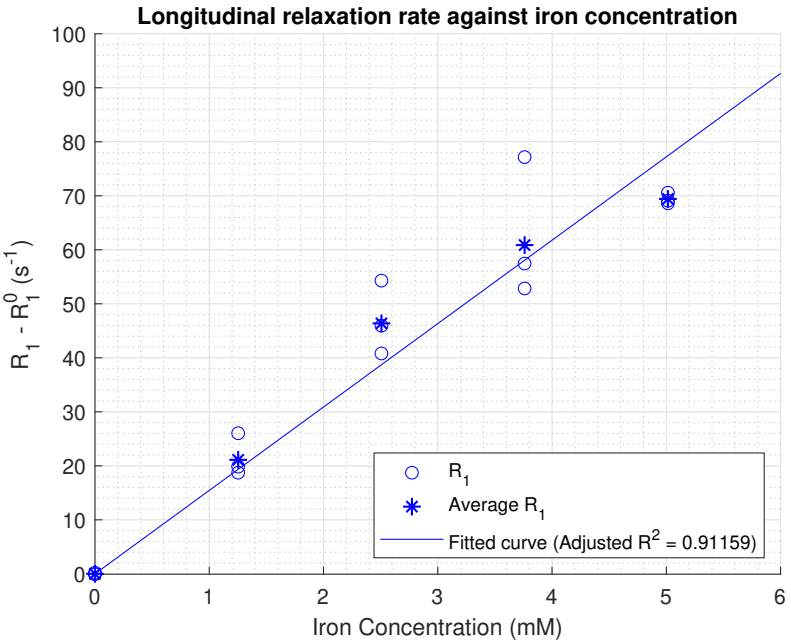

Figure 3: *The longitudinal relaxation rate for the corresponding concentrations, and the fit of the relaxivity*

Table 3 shows the iron concentration, the calculated iron concentration using R_1, and the calculated iron concentration using ΔR_1 of the Magtrace samples. That last calculation shows what the results would be if their concentration were determined using their relaxation rates, the native relaxation rate and the relaxivity.

Table 3: *Iron concentration of the sample and the calculated iron concentration using R_1 and the relaxivity*

Concentration	0%	0.25%	0.50%	0.75%	1.0%
Average R_1 (s^{-1})	0.253	21.4	46.7	61.2	69.7
Iron concentration (mM) [1]	0	1.253	2.507	3.760	5.014
Concentration using ΔR_1 [2]	0	1.39	3.03	3.98	4.53
Concentration using R_1 (mM) [3]	0.0229	1.39	3.03	3.98	4.35
Relative error between [2] and [1]	-	9.39%	20.1%	5.12%	-10.1%
Relative error between [3] and [1]	Inf	11.2%	21.0%	5.73%	-9.64%
Relative error between [2] and [3]	Inf	1.67%	0.76%	0.58%	0.51%
Absolute error between [2] and [3] (mM)	0.0229	0.0229	0.0229	0.0229	0.0229

The difference between the concentration calculated using R_1 and r_1 and the sample concentration is comparable to the error between the ΔR_1 concentration and the sample concentration. Both range from around -10% to around 20%. The relative error between the R_1 and the ΔR_1 concentrations are much smaller, between 1.67% and 0.51%. The absolute error stays the same, 0.0229 mM, which is equal to the iron concentration in the saline solution when it is calculated with its corresponding R_1 value and r_1. So, as the absolute error remains the same for all samples, the relative error decreases as R_1 increases.

3.3 Discussion

The differences in T_1 between the measurements of the same concentration can, among other things, be explained by the differences in temperature between the samples, as the relaxation time is temperature dependent. The tubes were mostly warmed up by the MRI scanner itself and not prior to acquisition, so the temperature was not the same between measurements. Warming the samples prior to acquisition to the temperature of the scanner (37°C) could have prevented this and would have increased the reliability and accuracy of the results, because then only the effect of the concentration on the relaxation time would have been taken into account.

Moreover, the choice on the amount of TIs is not backed by clear scientific evidence, as there is no consensus on the optimal number of TIs at which the signal intensity is measured. In this experiment, the suggested amount of TIs by Ogg, et al. was not used, as there was not guarantee that the T_1 of the samples would be less than 500 ms. The number suggested by Henoumont et al. was used instead, although there was not further information provided on whether or not more or less data points would lead to more or less accurate results, and on how the accuracy of the fit of T_1 was influenced by more or less data points.

3.3.1 Applicability on tracer quantification after an SLNB

It is important to note that the relaxivity of a tracer can differ when measured using different solvents, and that the degree of solvent dependency is not the same for every contrast agent or tracer. [46] For example, at 0.47 T and 37°C, Resovist (Schering, Berlin, Germany), a SPION based contrast agent, has a relaxivity of 20.6 ± 1.1 $s^{-1}mM^{-1}$ in water, but a relaxivity of 15 ± 1 $s^{-1}mM^{-1}$ in plasma. [46] This may also be the case for the relaxivity of Magtrace, so the measured relaxivity in water is not necessarily the same as the relaxivity in lymphatic tissue. Thus, using the calculated relaxivity to determine the concentration of the tracer in a lymph node could lead to an inaccurate quantification of the concentration.

A problem that remains in acquiring an accurate and reliable method to quantify the tracer concentration in an ex vivo lymph node, is the absence of a native T_1. However, the error that is made by calculating the concentration using R_1 instead of ΔR_1 does not seem to be very large; it equals the the concentration that is wrongly assigned by this method to the sample without any tracer. It is also constant over all samples. So, even though a quantitative analysis is not possible, a semi-quantitative seems realistic and possible.

However, a big difference between the experimental situation, with the tubes containing different tracer concentrations in the same solvent, and the clinical situation, with a lymph node containing Magtrace, remains. In the experimental situation, R_1^0 is the same for each sample, but this is not true for each voxel of a lymph node, as different lymphatic tissues have different relaxation times. [38, 39] Also, local differences in tissue composition could influence T_1. So the error that occurs by neglecting R_1^0 in calculating the concentration is not the same for every lymph node. In addition, the concentration would seem very different for two voxels with the same concentrations but with vastly different values for R_1^0. This problem is likely to occur in lymph nodes, because lymphatic tissues have quite different relaxation times; the cortex, hilum, and lymphatic fluid have T_1 relaxation times of around 1435, 714, and 3100, respectively. [38]

Another limitation in using this relaxivity in the case of an ex vivo lymph node, is that it is unknown which voxels contain Magtrace. Therefore, there is no way to know for which voxels the concentration actually has to be determined. Then, if all the relaxation rates would be divided by the relaxivity to determine the concentration, all voxels would be assigned a concentration, even if there is no tracer present, as Equation 3 assumes ΔR_1 and not R_1. If R_1^0 values were available, voxels containing no Magtrace would have a ΔR_1 of zero, so this problem would not occur.

3.4 Conclusion

In conclusion, the relaxivity of Magtrace, at around 37°C and a field strength of 0.5T, was measured to be 15.4 $s^{-1}mM^{-1}$. This is lower than the relaxivity of other SPION based tracers and contrast agents at similar field strengths, namely Resovist, SH U 555 C, and Feridex/Endorem (20.6 ±1.1, 23.9 ±1.2, and 27 ±1 $s^{-1}mM^{-1}$ at $B_0 = 0.47$T, respectively). [46] Using this relaxivity, the Magtrace concentration of a voxel can be calculated using its longitudinal relaxation time. However, there are some outliers in the measured

relaxation times, possibly caused by inconsistencies in the temperature of the tracers.

Further research is also needed to determine the relaxivity of Magtrace in lymphatic tissue, as the relaxivity is shown to be tissue specific. This knowledge would make the assessment of the Magtrace in lymphatic tissue more accurate. Also, more research could be done to determine an optimal amount of TIs that allows for both accurate and reliable results, and a manageable acquisition time, as there is no consensus in literature on what this amount is. This would hopefully lead to a more standardized and substantiated protocol on how to determine the relaxivity of a tracer.

4 Determining the tracer concentration of ex vivo lymph nodes using a T_1 map

4.1 Method

4.1.1 Data acquisition

The MR data was acquired using a 0.5 T MagSpec tabletop scanner from Pure Devices© (GmbH, Rimpar, Germany). The scanner operates at around 37°C. A 0D IRSE sequence was used, with TR set as five times the estimated T_1, as TR has to be sufficiently long to assure that the magnetizaton can return to equilibrium. [33, 35, 44] A map is made of the sample containing 0.25% Magtrace and of a lymph node from a breast cancer patient that was removed after an SLNB using Magtrace as a magnetic tracer as part of the LowMag trial (Christenhusz, et al., 2019). The used parameters are shown in Table 4.

Table 4: *MR parameters used for data acquisition*

	Magtrace sample (0.25%)	Lymph node
TE (s)	0.0050 s	0.0050 s
TI (s)	[0.0030, 0.0030, 0.0054, 0.0097, 0.0174, 0.0312, 0.0561, 0.1008, 0.1811, 0.3254, 0.5845, 1.0500]	[0.0050, 0.0050, 0.0988, 0.1925, 0.2863, 0.3800, 0.4738, 0.5675, 0.6613, 0.7550]
T_1 estimated (s)	0.035	1
TR	5*T_1 estimated	8*T_1 estimated
FOV	15x15 mm	14x14 mm
Resolution	4x4x1 voxels	28x28x1 voxels

4.1.2 T_1 fit

First, the signal intensity is normalized from -1 to 1 to get comparable ranges for the signal intensity and the inversion time and to decrease the sensitivity to ranging intitial values for the fit coefficients. Then, the data was fitted to Equation 1. The initial value for coefficient M_0 was derived by taking the absolute value of the signal intensity of the first data point, because, when using IRSE, its value equals M_0. When the data is normalized, M_0 equals -1. The intial value for T_1 was derived by finding the intersection between the curve through the data points and a line which equals 63% recovery to the equilibrium value (Figure 4). The initial value for a was set as zero.

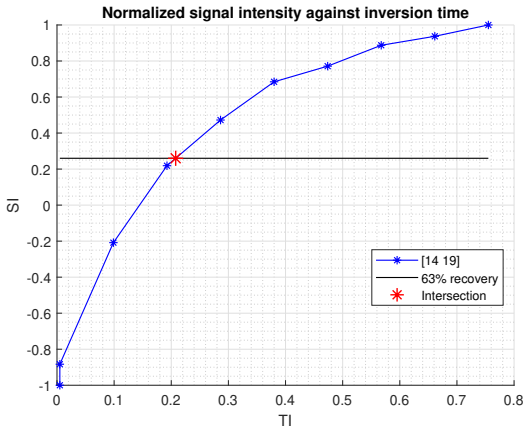

Figure 4: *Signal intensity, normalized between -1 and 1, against the inversion time. The initial value for T_1 is estimated by finding the intersection between the line through the data points and the line that corresponds to 63% recovery.*

Only signals originating from the lymph node or Magtrace sample should be mapped, so noise had to be removed. This was done in two steps. First, all data where the signal intensity at the first TI was higher than the signal intensity at the last TI was removed. Data originating from a voxel should follow a relaxation curve, where the signal intensity of the first data point is lower than that of the last one. So the data was

considered to be noise if this was not the case. Figure 5a shows data originating from a voxel, which does satisfy this condition, and Figure 5b shows noise, which does not satisfy the condition.

Second, all improbable values for T_1 were removed, as those were probably the result of fits done on noise that was not removed using the first condition. So all T_1 values equal to or less than zero, and greater than 400 ms was removed and not mapped.

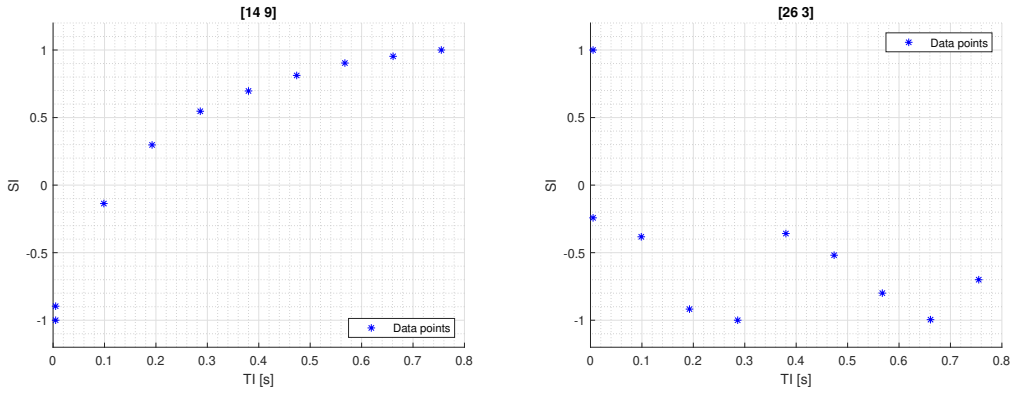

(a) *Normalized data, originating from a voxel in the lymph node. The data follows a relaxivity curve.*

(b) *Noise. There is no clear relaxation curve visible, so this data is not fitted.*

Figure 5

4.2 Results

4.2.1 T_1 map of the 0.25% Magtrace solution

The four by four map of the second slice of the 0.25% Magtrace solution is shown in Figure 7a. T_1 ranges from 61.6 ms to 63.8 ms, with an average T_1 of 62.8 ± 0.7 ms. The average T_1 over all slices is shown in Table 5. These values lie closely together, which is expected from a homogeneous solution. Also, the T_1 values of the voxels of each slice show little variation; the standard deviation is around one hundredth of the average T_1.

Table 5: *MR parameters used for data acquisition*

Slice	Average T_1 (ms)
1	63.0 ± 0.5
2	62.8 ± 0.7
3	62.7 ± 0.7
4	62.9 ± 0.6
Average over all slices	62.8 ± 0.6

The goodness of fit, quantified by the adjusted R^2 value, of each voxel of the slice mapped in Figure 7a is shown in Figure 7b. Adjusted R^2 is greater than 0.99 for each voxel. This is the case for all voxels across all slices. Also, visually evaluating the fit shows that the fit passes the fitted data points well (Figure 6).

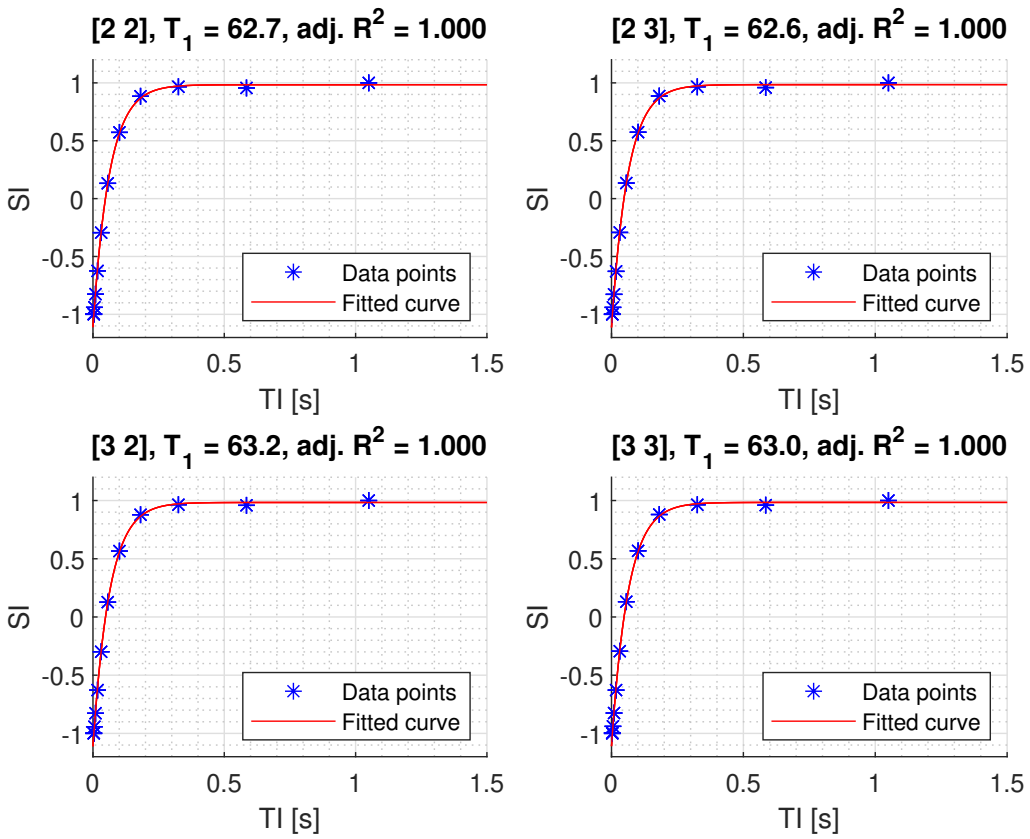

Figure 6: *Fit of four voxels of slice 2. The data was normalized between -1 and 1 prior to fitting. The fit follows the fitted data well, and the fit for all voxels has an adjusted R^2 of greater than 0.99.*

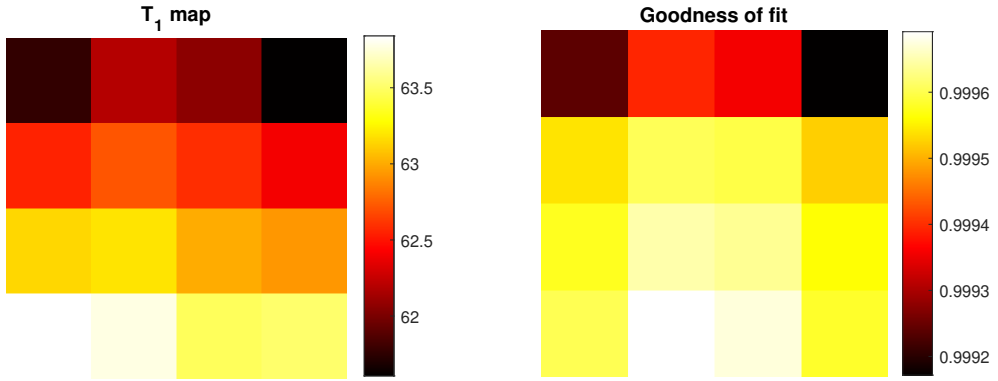

(a) *T_1 map of slice 2 of a four by four map of a Magtrace sample containing 0.25% Magtrace.*

(b) *Map of the goodness of fit of each voxel, expressed as the adjusted R^2 value, which is greater than 0.99 for each voxel.*

Figure 7: *Goodness of fit, quantified by the adjusted R^2, of the fit of Equation 1 to the data corresponding to the mapped voxels.*

What does stand out is that the derived T_1 differs significantly from the T_1 determined from the 0D measurements of the tube (Table 2). The average T_1 over three 0D measurements on the 0.25% Magtrace concentration was 46.6 ms, but the average T_1 over all four slices of the four by four map was 62.8 ms (Table 5).

4.2.2 T_1 map of the lymph node

The map of slice 16 of the lymph node and its corresponding map of the goodness of fit, quantified by the adjusted R^2 value, are shown in Figure 8a and Figure 8b, respectively. Adjusted R^2 is greater than 0.90 for 97% of the mapped voxels, and greater than 0.99 for 88% of the voxels. The goodness of fit is worse along the periphery of the mapped zone. A visual evaluation of the fits shows that it follows the fitted data points well (Figure 9).

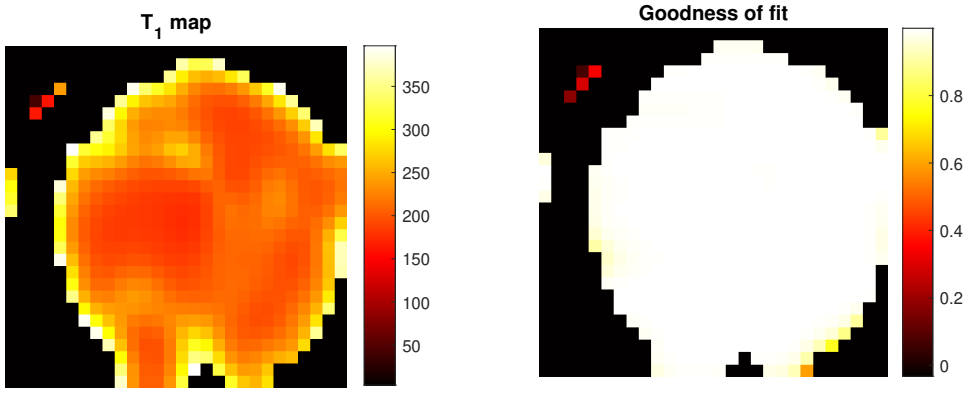

(a) *T_1 map of slice 16 of lymph node 2 of patient 55.*

(b) *Goodness of fit, quantified by the adjusted R^2, of the fit of Equation 1 to the data corresponding to the mapped voxels.*

Figure 8

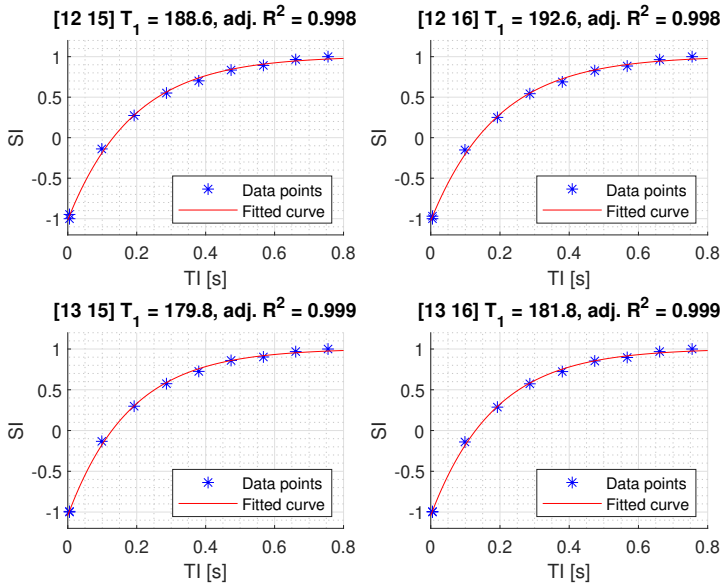

Figure 9: *Fit of four voxels of slice 16. The data was normalized between -1 and 1 prior to fitting. The fit follows the fitted data well, and the fit for all voxels has an adjusted R^2 of greater than 0.99.*

Results similar to that of slice 16 were the case for other slices (Figure 10). However, some voxels could not be mapped using this exact fitting method, as the fit got stuck in local minima or maxima, so it was not possible to map the entire lymph node. This issue was not solved within the time frame of the research. The slices do show similar ranges for T_1, from around 200 to 400 ms.

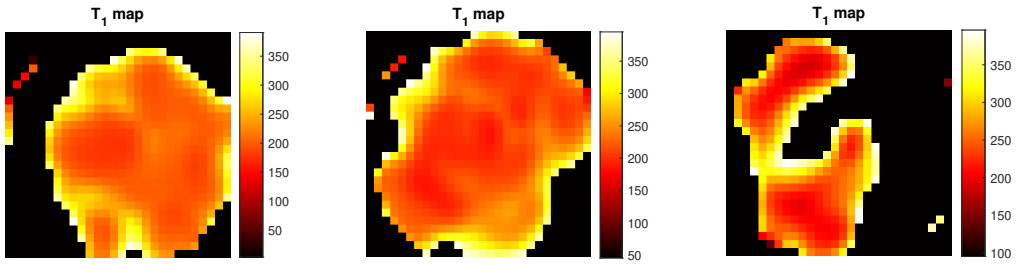

(a) T_1 *map of slice 15.* *(b)* T_1 *map of slice 19.* *(c)* T_1 *map of slice 28.*

Figure 10: T_1 *map of various slices of lymph node 2 of patient 55.*

4.3 Discussion

Normalizing the signal intensity between -1 and 1 prior to fitting helped in preventing the fit from approaching local minima and maxima. However, for some voxels this still happened and after this, fitting could not continue. Therefore, further data initialization and regularization, which prevents the model from getting stuck in local minima and maxima, is necessary.

Comparison to histopathology coupes could show more insight on the relation between the iron content of a voxel and its T_1 value. Based on the relaxivity, it is expected that T_1 in iron rich voxels would be lower than T_1 in voxels without any iron. Mapping more slices of more lymph nodes, and comparing those to histopathology coupes which visualize the tracer distribution could lead to a method to identify tracer rich voxels in a lymph node using only a post tracer admission T_1 map.

Also, the data acquisition of the lymph node was done using linearly spaced TIs, even though literature recommends logarithmically spread TIs in order to accurately map the first few moments after the inversion pulse, where the change in signal intensity is the largest. [31, 32, 33] In future acquisitions, this could be adjusted. The goodness of fit was already quite high for a majority of the voxels, so the gain in goodness of fit will probably not be a lot. However, the acquisition time could possibly be decreased if it were possible to get a similar goodness of fit using less, but logarithmically instead of linearly spaced, TIs. This could be useful pre- or intraoperative mapping of a lymph node, where time constraints are much stricter than for postoperative, ex vivo mapping.

Furthermore, the accuracy of the determined T_1 values could not be validated, as only tissues with unknown T_1 values were mapped. Validation could be done by mapping various materials with known T_1 values and evaluating the T_1 that results from the map. Moreover, the T_1 derived from the map of the Magtrace solution differs greatly from the T_1 derived from the 0D measurements. More maps need of more Magtrace samples can be made to identify the source of these differences. Also, materials with known T_1 values can be mapped to evaluate the differences the resulting relaxation times. Again, temperature differences between the samples at the time of acquisition could possibly have been the source, but this research cannot conclude whether or not that is the case.

4.3.1 Applicability on tracer quantification after an SLNB

The end goal would be to be able to assess the lymph node on the presence of metastases using only an MR map. However, a couple of factors prevent this currently. First, it is unknown what the differences are in MR properties between healthy lymphatic tissue and metastases originating from a breast tumor. Therefore, no distinction can be made between these two tissues using just an MR map. Second, although it is known how a magnetic tracer or contrast agent is generally distributed in a lymph node, it is unknown how it is distributed when there are metastases presence as well. [47] Knowledge about this could possibly help in identifying metastases in lymph nodes. Finally, there is no method available to identify which voxels in a lymph node contain tracer by only using a post tracer T_1 map. So this map does not give any information about that.

4.4 Conclusion

In conclusion, this section showed a fitting procedure to obtain a T_1 map of MR data of a sample containing a Magtrace solution and of a SPION enhanced lymph node of a breast cancer patient. In general, this method leads to a fit that follows the data points well, but there is no way to verify its accuracy and reliability, as only one fitting method was investigated.

This research does provide the necessary parts which can be used to determine the SPION concentration in an ex vivo sentinel lymph node - the relaxivity of the tracer and the T_1 map of a lymph node - but a quantitative assessment of the SPION concentration was not proven to be possible as of yet. Further research is needed to overcome the aforementioned obstacles that prevent this now. Also, to increase the applicability of the fit, further research is needed on data initialization and regularization, so that this fitting method could be applied to all voxels in all slices of every lymph node. Also, further research is needed to be able to quantitatively evaluate the lymph nodes on their tracer distribution, using the acquired T_1 maps and determined relaxivity. This could lead the way to an in vivo assessment of the presence of lymph nodes, which would eradicate the need to surgically remove lymph nodes from patients. Then, hopefully, using SPION-enhanced MR imaging, three quarters of SLNBs could be avoided in the future.

References

[1] Integraal Kankercentrum Nederland, "NKR Cijfers," 2022. [Online]. Available: https://iknl.nl/nkr-cijfers

[2] ——, "Overleving Borstkanker." [Online]. Available: https://iknl.nl/kankersoorten/borstkanker/registratie/overleving

[3] A. Chatterjee, N. Serniak, and B. Czerniecki, "Sentinel lymph node biopsy in breast cancer: A work in progress," *Cancer J.*, vol. 21, pp. 7–10, Jan-Feb 2015.

[4] F. Mettler and M. Guiberteau, *Essentials of Nuclear Medicine and Molecular Imaging*, seventh edition ed., F. A. Mettler and M. Guiberteau, Eds. Philadelphia: Elsevier, 2019.

[5] U. Veronesi, G. Viale, G. Paganelli, S. Zurrida, A. Luini, V. Galimberti, P. Veronesi, M. Intra, P. Maisonneuve, F. Zucca, G. Gatti, G. Mazzarol, C. De Cicco, and D. Vezzoli, "Sentinel lymph node biopsy in breast cancer: ten-year results of a randomized controlled study," *Ann Surg.*, vol. 251, pp. 595–600, Apr 2010.

[6] "Sentinel Lymph Node Biopsy," Aug. 2023, [Online; accessed 28. Aug. 2023]. [Online]. Available: https://www.cancer.gov/about-cancer/diagnosis-staging/staging/sentinel-node-biopsy-fact-sheet

[7] F. Rovera, F. Frattini, M. Marelli, A. D. Corben, G. Dionigi, L. Boni, and R. Dionigi, "Axillary sentinel lymph node biopsy: An overview," *International Journal of Surgery*, vol. 6, pp. S109–S112, Jan. 2008.

[8] P. Liu, J. Tan, Y. Song, K. Huang, Q. Zhang, and H. Xie, "The application of magnetic nanoparticles for sentinel lymph node detection in clinically node-negative breast cancer patients: A systemic review and meta-analysis," *Cancers*, vol. 14, Oct 2022.

[9] O. Ung, M. Tan, B. Chua, and B. Barraclough, "Complete axillary dissection: A technique that still has relevance in contemporary management of breast cancer," *ANZ Journal of Surgery*, vol. 76, pp. 518–521, Jun 2006.

[10] C. Bakri, N. Amalina, R. Kwasnicki, N. Khan, O. Ghandour, A. Lee, Y. Grant, A. Dawidziuk, D. Ara, H. Ashrafian, and D. Leff, "Impact of axillary lymph node dissection and sentinel lymph node biopsy on upper limb morbidity in breast cancer patients: A systematic review and meta-analysis," *Annals of Surgery*, vol. 277, pp. 572–580, Apr 2023.

[11] F. Petrelli, V. Lonati, and S. Barni, "Axillary dissection compared to sentinel node biopsy for the treatment of pathologically node-negative breast cancer: a meta-analysis of four randomized trials with long-term follow up," *Oncology Reviews*, vol. 6, no. 2, Oct. 2012.

[12] T. Alsumai, N. Alhazzaa, A. Alshamrani, S. Assiri, and A. Alhefdi, "Factors predicting positive sentinel lymph node biopsy in clinically node-negative breast cancer," *Breast Cancer (Dove Med Press)*, vol. 14, pp. 323–334, May 2022.

[13] kanker.nl, "Schildwachtklierprocedure bij borstkanker." [Online]. Available: https://www.kanker.nl/kankersoorten/borstkanker/behandelingen/schildwachtklierprocedure-bij-borstkanker

[14] "Sentinel Lymph Node Biopsy," Sep. 2023, [Online; accessed 28. Sep. 2023]. [Online]. Available: https://www.cancer.gov/about-cancer/diagnosis-staging/staging/sentinel-node-biopsy-fact-sheet#what-are-the-possible-harms-of-slnb

[15] J. Tollefson, "Reactor shutdown threatens world's medical-isotope supply," *Nature*, Sep 2016.

[16] S. Shams, K. Lippold, J. U. Blohmer, R. Röhle, F. Kühn, and M. M. Karsten, "A Pilot Study Evaluating the Effects of Magtrace® for Sentinel Node Biopsy in Breast Cancer Patients Regarding Care Process Optimization, Reimbursement, Surgical Time, and Patient Comfort Compared With Standard Technetium99," *Annals of Surgical Oncology*, vol. 28, no. 6, p. 3232, 2021.

[17] J. Pouw, M. Grootendorst, R. Bezooijen, C. Klazen, W. De Bruin, J. Klaase, M. Hall-Craggs, M. Douek, and B. Ten Haken, "Pre-operative sentinel lymph node localization in breast cancer with superparamagnetic iron oxide mri: the sentimag multicentre trial imaging subprotocol," *The British journal of radiology*, vol. 88, 2015.

[18] E. Wilbrink-Winkelhorst, "Optimisation of the magnetic procedure to detect the sentinel lymph node in breast cancer patients," pp. 67–81, 2020.

[19] R. Freeman, *Medical Imaging Signals and Systems*. Pearson Education, 2006.

[20] T. Kagawa, S. Yoshida, T. Shiraishi, M. Hashimoto, D. Inadomi, M. Sato, T. Tsuzuki, K. Miwa, and K. Yuasa, "Basic principles of magnetic resonance imaging for beginner oral and maxillofacial radiologists," *Oral Radiology*, vol. 33, no. 2, pp. 92–100, May 2017.

[21] R.-J. M. van Geuns, P. A. Wielopolski, H. G. de Bruin, B. J. Rensing, P. M. A. van Ooijen, M. Hulshoff, M. Oudkerk, and P. J. de Feyter, "Basic principles of magnetic resonance imaging," *Progress in Cardiovascular Diseases*, vol. 42, no. 2, pp. 149–156, Sep. 1999.

[22] A. Taylor, M. Salerno, R. Dharmakumar, and M. Jerosch-Herold, "T1 mapping: Basic techniques and clinical applications," *JACC: Cardiovascular Imaging*, vol. 9, pp. 67–81, 2016.

[23] A. Elster, "T1 relaxation: Definition."

[24] S. Rao, S. Tseng, A. Pednekar, S. Siddiqui, M. Kocaoglu, M. Fares, S. Lang, S. Kutty, A. Christopher, L. Olivieri, M. Taylor, and T. Alsaied, "Myocardial parametric mapping by cardiac magnetic resonance imaging in pediatric cardiology and congenital heart disease," *Circulation: Cardiovascular Imaging*, vol. 15, Jan 2022.

[25] K. Wieriks, "The possibility of superparamagnetic iron oxide nanoparticles as positive contrast agents in low-field mra," 2022.

[26] H.-L. M. Cheng, N. Stikov, N. R. Ghugre, and G. A. Wright, "Practical medical applications of quantitative MR relaxometry," *Journal of Magnetic Resonance Imaging*, vol. 36, no. 4, pp. 805–824, Oct. 2012.

[27] P. Haaf, P. Garg, D. R. Messroghli, D. A. Broadbent, J. P. Greenwood, and S. Plein, "Cardiac T1 Mapping and Extracellular Volume (ECV) in clinical practice: a comprehensive review," *Journal of Cardiovascular Magnetic Resonance*, vol. 18, no. 1, pp. 1–12, Jan. 2017.

[28] J. O. S. H. Cleary and A. R. Guimarães, "Magnetic Resonance Imaging," in *Pathobiology of Human Disease*. Cambridge, MA, USA: Academic Press, Jan. 2014, pp. 3987–4004.

[29] R. Freeman, *Magnetic Resonance in Chemistry and Medicine*. Oxford University Press, 2003.

[30] V. Jacques, S. Dumas, W. Sun, J. Troughton, M. Greenfield, and P. Caravan, "High relaxivity mri contrast agents part 2: Optimization of inner- and second-sphere relaxivity," *Invest Radiol.*, vol. 45, pp. 613–624, Oct 2011.

[31] Y. Shen, F. L. Goerner, C. Snyder, J. N. Morelli, D. Hao, D. Hu, X. Li, and V. M. Runge, "T1 relaxivities of gadolinium-based magnetic resonance contrast agents in human whole blood at 1.5, 3, and 7 T," *Investigative Radiology*, vol. 50, no. 5, pp. 330–338, May 2015.

[32] A. D. Bain, "The choice of parameters in an nmr experiment. application to the inversion-recovery t1 method," *Journal of Magnetic Resonance (1969)*, vol. 89, no. 1, pp. 153–160, 1990. [Online]. Available: https://www.sciencedirect.com/science/article/pii/002223649090170E

[33] C. Henoumont, S. Laurent, and L. Vander Elst, "How to perform accurate and reliablemeasurements of longitudinal and transverserelaxation times of mri contrast media inaqueous solutions," *Contrast Media & Molecular Imaging*, vol. 4, pp. 312–321, 2009.

[34] R. Ogg and P. Kingsley, "Optimized precision of inversion-recovery t1 measurements for contrained scan time," *Magnetic Resonance in Medicine*, vol. 51, pp. 625–630, Feb 2004.

[35] J. Burt, S. Zimmerman, I. Kamel, M. Halushka, and D. Bluemke, "Myocardial t1 mapping: Techniques and potential applications," *Radiographics*, vol. 34, pp. 377–95, Mar-Apr 2014.

[36] C. E. Anderson, M. Johansen, B. O. Erokwu, H. Hu, Y. Gu, Y. Zhang, M. Kavran, J. Vincent, M. L. Drumm, M. A. Griswold, N. F. Steinmetz, M. Li, H. Clark, R. J. Darrah, X. Yu, S. M. Brady-Kalnay, and C. A. Flask, "Dynamic, Simultaneous Concentration Mapping of Multiple MRI Contrast Agents with Dual Contrast - Magnetic Resonance Fingerprinting," *Scientific Reports*, vol. 9, no. 19888, pp. 1–11, Dec. 2019.

[37] Y. Matsumoto, M. Harada, Y. Kanazawa, Y. Taniguchi, M. Ono, and Y. Bito, "Quantitative parameter mapping of contrast agent concentration and relaxivity and brain tumor extracellular pH," *Scientific Reports*, vol. 12, 2022.

[38] R. Crescenzi, P. M. Donahue, V. G. Braxton, A. O. Scott, H. B. Mahany, S. K. Lants, and M. J. Donahue, "3.0T relaxation time measurements of human lymph nodes in adults with and without lymphatic insufficiency: implications for magnetic resonance lymphatic imaging," *NMR in biomedicine*, vol. 31, no. 12, p. e4009, Dec. 2018.

[39] S. Rane, P. M. C. Donahue, T. Towse, S. Ridner, M. Chappell, J. Jordi, J. Gore, and M. J. Donahue, "Clinical feasibility of noninvasive visualization of lymphatic flow with principles of spin labeling MR imaging: implications for lymphedema assessment," *Radiology*, vol. 269, no. 3, pp. 893–902, Dec. 2013.

[40] Jul. 2018, [Online; accessed 24. May 2023]. [Online]. Available: https://www.accessdata.fda.gov/cdrh_docs/pdf16/P160053D.pdf

[41] Jul. 2018, [Online; accessed 24. May 2023]. [Online]. Available: https://www.accessdata.fda.gov/cdrh_docs/pdf16/P160053B.pdf

[42] PubChem, "Carboxydextran," Jun. 2023, [Online; accessed 8. Jun. 2023]. [Online]. Available: https://pubchem.ncbi.nlm.nih.gov/compound/Carboxydextran

[43] J. De Laeter, J. Böhlke, P. De Bièvre, H. Hidaka, H. Peiser, K. Rosman, and P. Taylor, "Atomic weights of the elements: review 2000," *Pure Appl. Chem*, vol. 75, no. 6, pp. 683–800, 2003. [Online]. Available: https://www.ciaaw.org/pubs/EXER-2000.pdf

[44] I. Reyes-Molina, A. Hernández-Rodríguez, C. Cabal-Mirabal, and E. Gonzalez-Dalmau, "Methodology for determination of contrast agent relaxivity using mri," nov 2022.

[45] T. M. Inc., "Matlab version: 9.11.0.1809720 (r2021b) update 1," Natick, Massachusetts, United States, 2021. [Online]. Available: https://www.mathworks.com

[46] M. Rohrer, H. Bauer, J. Mintorovitch, M. Requardt, and H. Wienmann, "Comparison of Magnetic Properties of MRI Contrast Media Solutions at Different Magnetic Field Strengths," *Investigative Radiology*, vol. 240, no. 11, pp. 715–724, Nov. 2005.

[47] L. Johnson, S. E. Pinder, and M. Douek, "Deposition of superparamagnetic iron-oxide nanoparticles in axillary sentinel lymph nodes following subcutaneous injection," *Histopathology*, vol. 62, no. 3, pp. 481–486, Feb. 2013.